Journal of Radioanalytical and Nuclear Chemistry (2022) 331:3965–3977
https://doi.org/10.1007/s10967-022-08426-7

Adsorption performance of sulfonamide-modified metal–organic frameworks (MOFs) for Co(II) in aqueous solution

Yipeng Zhou[1] · Xiaowei Wang[1] · Jinfeng Men[1] · Mingchun Jia[1] · Chengqiang Liang[1]

Received: 22 April 2022 / Accepted: 29 June 2022 / Published online: 26 August 2022

Abstract

Efficient treatment of cobalt ions from mining wastewater and effluents from nuclear facilities is critical for environmental protection. A zeolite imidazole frameworks (ZIFs), which belong to a metal–organic frameworks (MOFs), was successfully synthesized and functionalized with sulfonamide to obtain a ZIF-90-SO_2HN_2 with high-efficiency adsorption of cobalt ions. The synthesized material was characterized by scanning electron microscopy, thermogravimetric analysis, N_2 adsorption–desorption, X-ray diffraction and Fourier transform infrared spectroscopy. The adsorption performance of ZIF-90-SO_2HN_2 for Co(II) in simulated wastewater was studied. The synthesized ZIF-90-SO_2HN_2 has a maximum adsorption capacity of about 122.85 mg g^{-1} for Co(II) under the conditions of pH = 6.72 and T = 303 K with an initial solution concentration of 250 mg L^{-1}. The adsorption equilibrium time is about 120 min. ZIF-90-SO_2HN_2 exhibits selective adsorption of Co(II) and Ni(II) in multi-metal ion solution. Thermodynamic and kinetic analysis reflects that the adsorption process of Co(II) by ZIF-90-SO_2HN_2 is spontaneous and endothermic, which is consistent with pseudo-second-order chemisorption and Langmuir monolayer adsorption.

Keywords Cobalt · Metal organic frameworks · Adsorption · Thermodynamic · Kinetic · Isotherm

Introduction

In the process of industrial waste liquid discharge, water pollution caused by toxic heavy metals is a ubiquitous environmental crisis. Heavy metal pollution of wastewater can cause many health problems for plants, animals and humans. Therefore, it is necessary to separate these heavy metal ions from wastewater. Among them, the pollution of cobalt is of significant importance, because this metal is not only used in mining, metallurgy, pigments and electronics, but also exists in the wastewater of nuclear facilities [1]. As cobalt is a highly toxic metal, excessive intake of cobalt can cause diseases such as asthma, allergies, heart failure, liver and thyroid damage [2]. If radioactive ^{60}Co is ingested, it would further cause aplastic anemia and leukemia [3]. Therefore, it is crucial to deal with the water pollution by removing cobalt from wastewater. There are several methods for removing cobalt from wastewater, which include adsorption [4], chemical precipitation [5], reverse osmosis [6] and ion exchange [7]. Compared with the other treatment methods, the advantages of adsorption method are simple process design and operation, low separation cost and high selectivity [8]. Traditional adsorbents such as clay minerals, resins, biochar, oxides and other materials are widely used in the removal of cobalt ions [9–11]. However, the application of these adsorbents is still limited due to low adsorption capacity, poor selectivity and structural instability [12]. Therefore, there is an urgent need to develop a more efficient selective material to adsorb cobalt ions in wastewater.

Metal–organic frameworks (MOFs) are typical crystalline porous materials composed of metals (clusters) and organic linkers connected by coordination, which have both the rigidity of inorganic materials and the flexibility of organic materials [13]. In recent years, MOFs have been widely used in gas storage [14, 15], drug dilution [16, 17], catalysis [18, 19], sensing [20, 21], separation [22, 23] and other fields due to their high specific surface area and easy-to-modify structure. As a representative series of MOFs, zeolite imidazole frameworks (ZIFs) are assembled with Zn(II) or Co(II) as the metal source and imidazole and its derivatives as the organic ligands [24]. ZIF-90 is composed

✉ Xiaowei Wang
actwang@sina.com

[1] Naval University of Engineering, Wuhan, China

of Zn(II) coordinated with imidazole-2-carbaldehyde, which has excellent hydrophilicity and stability [25]. The –CHO group on its backbone is easy to be modified and the pi-acceptor properties of the imine nitrogen makes it possible to graft onto ZIF-90 via the Schiff base reaction [26]. ZIF-90 modified by this method has great potential in the adsorption of metal ions [27, 28], organics [29] and gases [30]. The successful application in a variety of chelated heavy metal ions [31, 32] reflects the feasibility of the Schiff base reaction. According to the soft and hard acid–base theory [33], Co(II) may have more binding sites with the sulfonamide group as a junctional acid. Therefore, grafting sulfonamide onto ZIF-90 via Schiff base reaction may have better adsorption effect on Co(II).

In this study, we synthesized a novel sulfonamide-modified MOF material, ZIF-90-SO_2HN_2, for the capture and removal of Co(II) from simulated wastewater at the ppm level. The adsorption properties of ZIF-90 and ZIF-90-SO_2HN_2 for Co(II) in solution under different conditions were studied. The isotherms and kinetics of the adsorption process were analyzed, and the adsorption mechanism of the whole process was discussed, the application of ZIF-90-SO_2HN_2 adsorption treatment of Co(II) in wastewater was beneficially explored.

Experimental section

Reagents and apparatus

All purchased chemicals were used as received without further purification. Anhydrous methanol (CH_3OH) was purchased from Tianjin Youpu Chemical Technology Co., Ltd. Dimethylformamide (C_3N_7NO) was purchased from Tianjin Comeo Chemical Reagent Co., Ltd. Imidazole-2-carbaldehyde ($C_4H_4N_2O$) and Sulfonamide ($C_4H_8N_2O_2S$) were purchased from Shanghai Yien Chemical Technology Co., Ltd. All metal nitrates, metal chlorides, hydrochloric acid, NaOH purchased from Tianjin Damao Chemical Reagent Co., Ltd.

XRD patterns of the materials were carried out using a D8 DISCOVER GADDS X-ray diffractometer produced by BRUKER AXS Corporation (USA) with a CuKα radiation at 40 kV and 30 mA and data were collected between 5°and 50°. The thermal stability of the sample was tested under nitrogen atmosphere with STA409 PC/PG thermogravimetric analyzer produced by NETZSCH Corporation (Germany). The morphology of the material was observed by Gemini 500 field emission scanning electron microscope produced by ZEISS Corporation (Germany). The specific surface area and pore volume of the sample was measured by N_2 adsorption–desorption method on ASAP 2020 PLUS H specific surface and porosity analyzer produced by MICROMERITICS Corporation (USA). The concentration of Co(II) was analyzed with the ContrAA700 atomic absorption spectrophotometer manufactured by Analytik Jena AG (Germany).

Synthesis of ZIF-90

ZIF-90 were synthesized in DMF system, and the specific process is as follows [34]: 0.81 g imidazole-2-carbaldehyde and 0.75 g zinc nitrate were added into 30 mL dimethylformamide, stirred at 80 °C for 2 h until the solution is completely clear, then cool to room temperature. 20 mL of methanol and 0.2 mL of ammonia water were pour into the mixed solution at the same time, and stirred rapidly for 2 h. The resulting precipitate was centrifuged and washed three times with anhydrous methanol to remove zinc nitrate and imidazole-2-carbaldehyde that did not participate in the reaction. The washed product was placed in a vacuum drying box, dried under vacuum at 100 °C for 12 h to remove methanol molecules and water molecules in the pores, and finally obtained a yellow powder ZIF-90.

Synthesis of ZIF-90-SO_2HN_2

The specific synthesis process of ZIF-90-SO_2HN_2 is as follows: 0.50 g of dried ZIF-90 and 0.67 g of sulfonamide were added to 50 mL of anhydrous methanol solution, and the reaction was stirred at 80 °C for 12 h. The resulting pale yellow precipitate was centrifuged and washed three times with anhydrous methanol to remove unreacted sulfonamide. The washed product was vacuum-dried at 100 °C for 12 h to remove methanol molecules and water molecules in the pores. The final obtained light yellow powder was ZIF-90-SO_2HN_2. The overall synthetic route is shown in Fig. 1.

Adsorption experiments

In the adsorption experiment, the dosage of metal ion solution was 0.05L, and the dosage of adsorbents ZIF-90 and ZIF-90-SO_2HN_2 were both 0.02 g. Adjust the pH of the solution with 0.5 mol L^{-1} HCl or NaOH solution. After adsorption, the supernatant was taken for ion concentration detection. The adsorption capacity of the adsorbent for Co(II) is calculated by formula (1):

$$Q_t = \frac{C_0 - C_t}{m} \times V \quad (1)$$

where C_0 is the initial concentration of the metal ion (mg L^{-1}), C_t is the residual concentration of the metal ion (mg L^{-1}), V is the volume of the testing solution (L), m is the mass of the adsorbent (g).

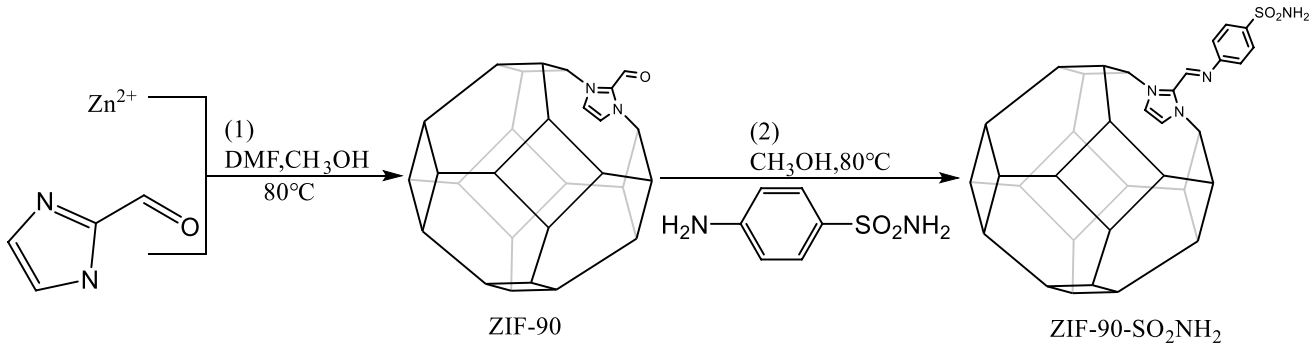

Fig. 1 Synthesis flow chart of ZIF-90-SO_2HN_2

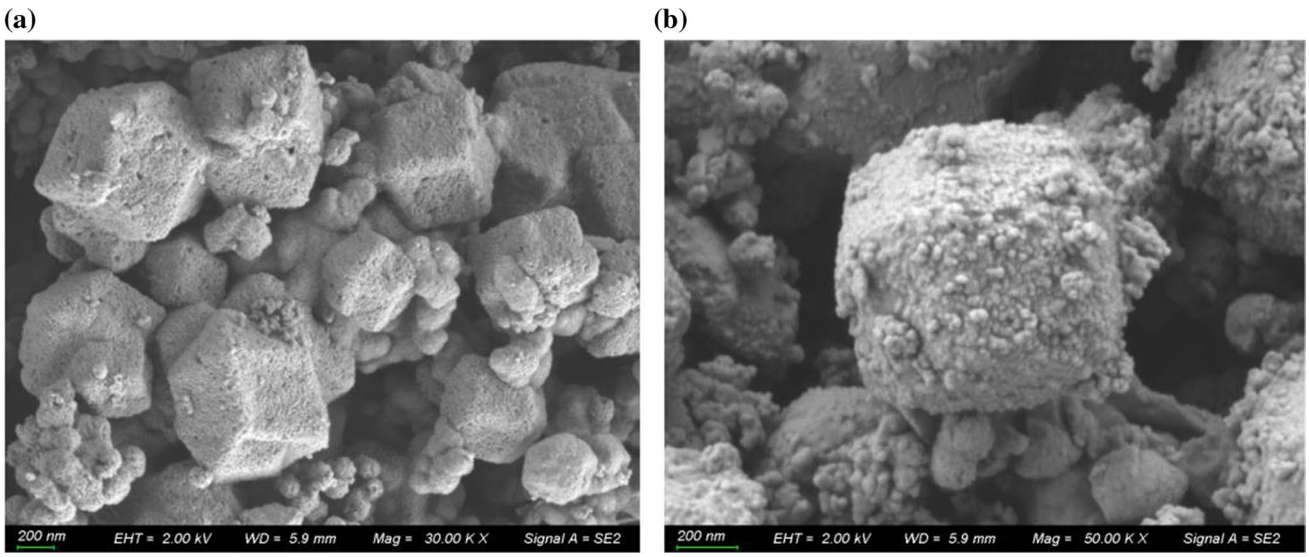

Fig. 2 SEM image of ZIF-90 (**a**) and ZIF-90-SO_2HN_2 (**b**) sample

Results and discussions

Characterization

The experimentally prepared ZIF-90 and ZIF-90-SO_2HN_2 are fine powder particles, and the SEM images of the two are shown in Fig. 2. It can be seen that the average crystal particle size of the obtained ZIF-90 and ZIF-90-SO_2HN_2 is less than 1 μm, The surface of ZIF-90-SO_2HN_2 is rougher than that of ZIF-90, which indicates that the sulfonamide group was successfully grafted on ZIF-90.

The XRD test results of ZIF-90 and ZIF-90-SO_2HN_2 are shown in Fig. 3. It can be seen that the characteristic peaks corresponding to the XRD obtained by the experimentally prepared ZIF-90 test are consistent with the characteristic peaks corresponding to ZIF-90 in other literatures [35]. There are 6 main diffraction peaks around 7.24°, 10.24°, 12.54°, 14.48°, 16.22°and 17.78°, corresponding to (011),

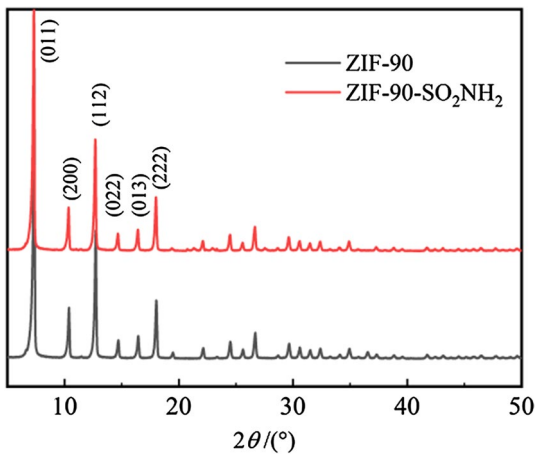

Fig. 3 XRD pattern of ZIF-90 and ZIF-90-SO_2HN_2

(200), (112), (022), (013) and (222), which indicates the successful formation of the ZIF-90 crystal structure. The structure of the ZIF-90 framework is related to the sodalite (SOD) topology in zeolites, showing an extended three-dimensional network [30]. All characteristic peaks of ZIF-90-SO_2HN_2 and ZIF-90 are consistent, indicating that the original structure of the material did not change after grafting sulfonamide.

The thermal stability of ZIF-90 and ZIF-90-SO_2HN_2 was tested by TGA under nitrogen atmosphere, the heating rate was controlled at 10 °C min^{-1}, and the temperature range was controlled within 25–1000 °C. The results are shown in Fig. 4. At 110 °C, the weight loss of ZIF-90-SO_2HN_2 is about 4.24%, which is due to the detachment of methanol molecules or water molecules with lower boiling points from the surface or cavity of the crystal. When the temperature reaches about 300 °C, the mass of the sample decreases by 9.74%, which is because the higher boiling DMF molecules in ZIF-90-SO_2HN_2 are detached from the cavity of the crystal [34]. When the temperature reaches 1000 °C, the bonds in the organic molecular chain of the material are pyrolyzed by high temperature, and the metal ions are also volatilized, and finally inorganic carbon is left [36].

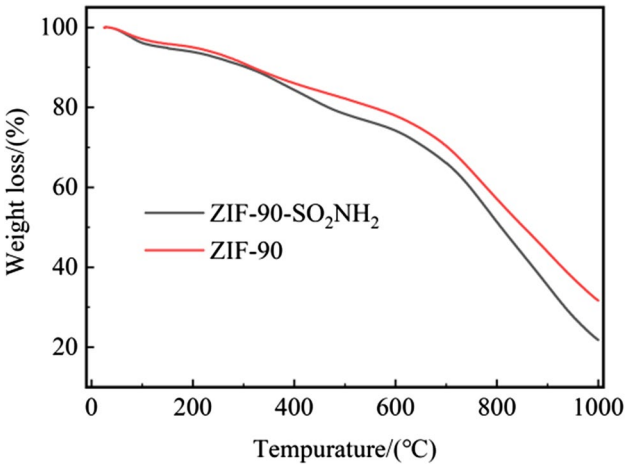

Fig. 4 TGA curve of ZIF-90 and ZIF-90-SO_2HN_2

Figure 5 shows the N_2 adsorption–desorption isotherms and pore size distribution of ZIF-90 and ZIF-90-SO_2HN_2. It can be seen that the adsorption isotherms of both are belong to the type I isotherm [37], indicating that ZIF-90 and ZIF-90-SO_2HN_2 are typical microporous materials. The BET specific surface areas of the two are 640.82m^2 g^{-1} and 59.56m^2 g^{-1} respectively. The smaller specific surface area of ZIF-90-SO_2HN_2 is because the successful grafting of sulfonamide groups occupies a large number of pores. The pore size of ZIF-90 is distributed in the range of 0.80–1.00 nm, and that of ZIF-90-SO_2HN_2 is in the range of 1.09–1.18 nm, both of which belong to the microporous structure, which is consistent with the results of N_2 adsorption.

The results of the FTIR assay analysis of ZIF-90 and ZIF-90-SO_2HN_2 are shown in Fig. 6. The representative peak of ZIF-90 at 1675 cm^{-1} is caused by the –CHO moiety [38], and the bond at 2855 cm^{-1} is the C-H stretching vibration in C–CHO [39]. Compared with ZIF-90, ZIF-90-SO_2HN_2 showed three new peaks at 1635 cm^{-1}, 1510 cm^{-1} and 1124 cm^{-1} in the FTIR spectrum. The peak at 1630 cm^{-1} may be the stretching vibration of the imine C=N generated by the dehydration condensation of the aldehyde group and the amino group [40]. The peak at 1510 cm^{-1} may correspond to the stretching vibration of C–C in the benzene ring in the sulfonamide group [27]. The peak at 1124 cm^{-1} may correspond to the symmetric stretching vibration of O=S=O [41]. These results indicate that the sulfonamide groups have been successfully grafted onto ZIF-90.

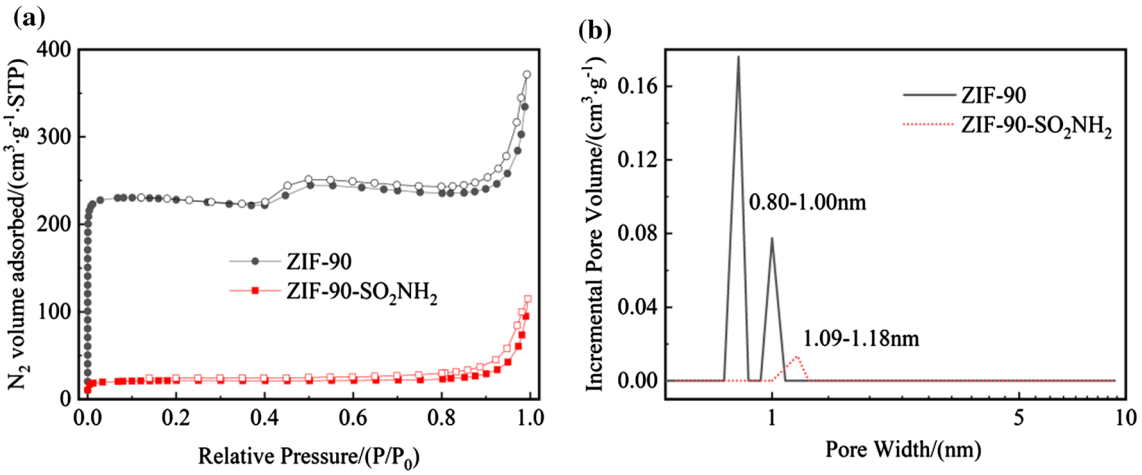

Fig. 5 N_2 adsorption–desorption isotherm (**a**) and pore size distribution (**b**) of ZIF-90 and ZIF-90-SO_2HN_2

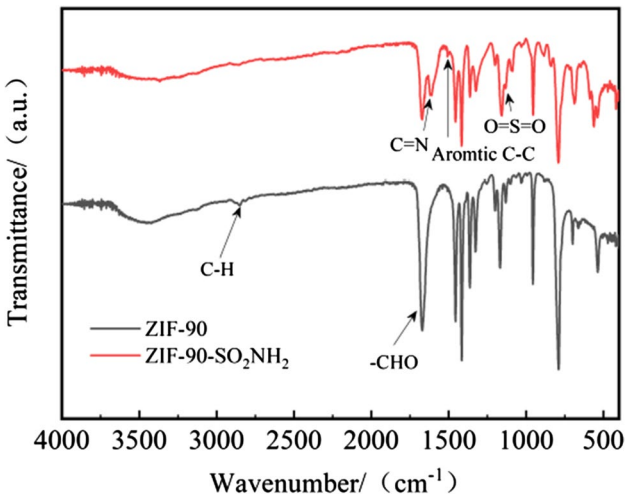

Fig. 6 FTIR pattern of ZIF-90 and ZIF-90-SO_2HN_2

Effect of pH

The initial pH value of the solution not only affects the dissociation equilibrium of Co(II) in aqueous solution, but also affects the adsorption effect of the adsorbent. To determine the optimum adsorption pH value, the pH range of the experiment was set to 3.0–8.0, the adsorption time was set to 24 h, the initial concentration of Co(II) in the solution was 10 mg L^{-1}, and the reaction temperature was 303 K. The effect of pH on ZIF-90 and ZIF-90-SO_2HN_2 adsorption performance is shown in Fig. 7a. the adsorption capacity of ZIF-90 and ZIF-90-SO_2HN_2 for Co(II) increased gradually with the increase of pH. When pH = 6.0, ZIF-90 has the best adsorption effect on Co(II) with the adsorption capacity is 6.99 mg L^{-1}; When pH = 7.0, ZIF-90-SO_2HN_2 has the best adsorption effect on Co(II), and the adsorption capacity is 13.72 mg L^{-1}. The poor adsorption of Co(II) by ZIF-90 and ZIF-90-SO_2HN_2 in acidic environment is due to the competitive adsorption of protons. The decrease of the adsorption capacity in an alkaline environment is because the hydrolysis and polymerization of Co(II) in the solution is enhanced, resulting in the formation of colloidal clusters with hydroxyl groups with a larger radius, and the microporous structure of the adsorbent cannot completely adsorb these colloidal clusters. The speciation of cobalt at different pH was simulated with Hydra and Medusa software, and the results are shown in Fig. 7b. It can be observed that a small amount of $CoOH^+$, dissolved $Co(OH)_2$ and solid $Co(OH)_2$ will be produced in the pH range of 7.0–8.0, which will have an adverse effect on the adsorption of cobalt on the adsorbent, which further corroborates the experimental results.

Effect of contact time

The adsorption capacity of ZIF-90 and ZIF-90-SO_2HN_2 for Co(II) with time is shown in Fig. 8. The results showed that ZIF-90 reached equilibrium at about 100 min, and the adsorption capacity was 6.98 mg g^{-1}; ZIF-90-SO_2HN_2 basically reached equilibrium at about 120 min, and the equilibrium adsorption capacity was 13.02 mg g^{-1}.

Analysis of adsorption kinetics provides a clearer understanding of the behavior of the adsorption process. The adsorption process was analyzed using the Lagergren pseudo-first-order kinetic model and pseudo-second-order kinetic model. The expressions for the two models are as follows[42]:

$$\ln\left(Q_e - Q_t\right) = \ln Q_e - K_1 t \tag{2}$$

$$\frac{t}{Q_t} = \frac{1}{K_2 Q_e^2} + \frac{t}{Q_e} \tag{3}$$

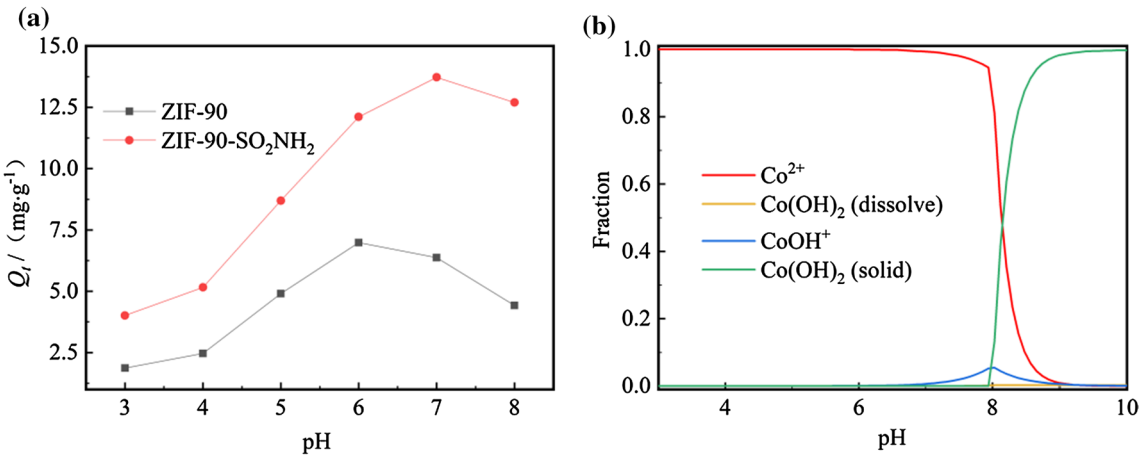

Fig. 7 **a** The curve of the adsorption capacity of ZIF-90 and ZIF-90-SO_2HN_2 with the change of pH; **b** Speciation of cobalt at different pH (T = 303 K, initial Co(II) concentration of 10 mg $g.^{-1}$, t = 720 min)

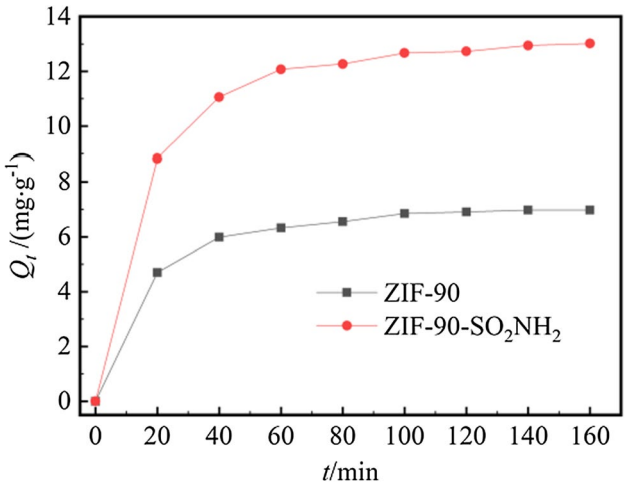

Fig. 8 The change curve of ZIF-90 and ZIF-90-SO_2HN_2 adsorption capacity with adsorption time (pH = 6.67, T = 303 K, initial Co(II) concentration of 10 mg L^{-1})

where Q_e is the equilibrium adsorption capacity (mg g^{-1}); K_1 is the pseudo-first-order kinetic rate constant (min^{-1}); K_2 is the pseudo-second-order kinetic rate constant (g mg^{-1} min^{-1}).

The adsorption capacities of ZIF-90 and ZIF-90-SO_2HN_2 at different times were fitted with two kinetic models, and the results are shown in Fig. 9 and Table 1. It can be seen that the pseudo-second-order kinetic model has better fitting results than the pseudo-first-order kinetic model. The equilibrium adsorption capacities of ZIF-90 and ZIF-90-SO_2HN_2 for Co(II) calculated by the pseudo-second-order kinetic model are 7.58 mg g^{-1} and 13.89 mg g^{-1}, respectively, which are close to the experimental results. Therefore, it can be determined that the adsorption process of Co(II) by ZIF-90 and ZIF-90-SO_2HN_2 is chemical adsorption.

In addition, the initial adsorption rate and half-adsorption time of the adsorbent can be calculated from the pseudo-second-order rate constant as follows [43]:

$$h = K_2 Q_e^2 \tag{4}$$

$$t_{1/2} = \frac{1}{K_2 Q_e} \tag{5}$$

where h is the initial adsorption rate when $t \to 0$ (mg g^{-1} min^{-1}); $t_{1/2}$ is the time required for the adsorption capacity to reach half of the equilibrium adsorption capacity

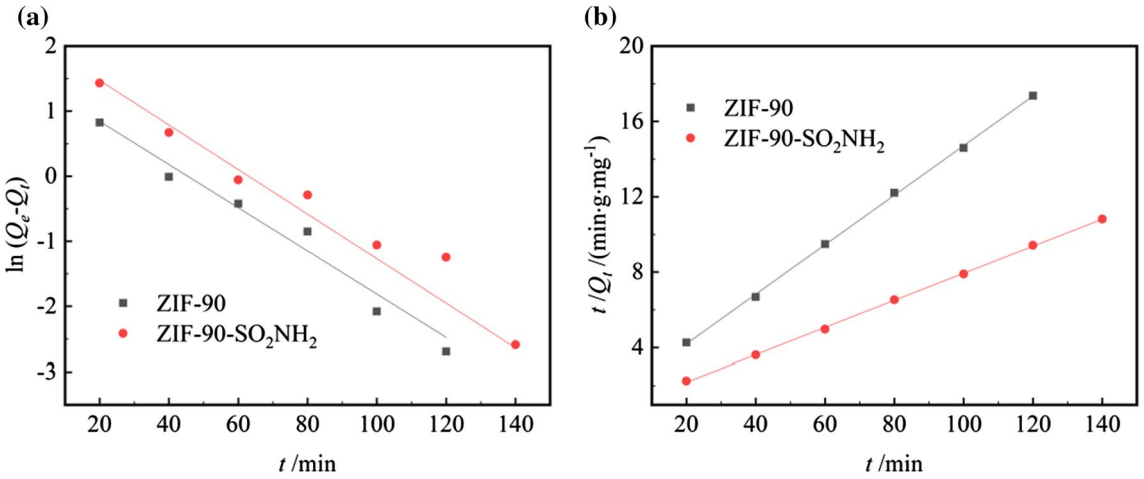

Fig. 9 Pseudo-first-order (**a**) and pseudo-second-order (**b**) kinetic fitting of ZIF-90 and ZIF-90-SO_2HN_2 (pH = 6.67, T = 303 K, initial Co(II) concentration of 10 mg L^{-1})

Table 1 Fitting parameters of ZIF-90 and ZIF-90-SO_2HN_2 adsorption kinetic model (pH = 6.67, T = 303 K, initial Co(II) concentration of 10 mg L^{-1})

Kind of adsorbent	Pseudo-first-order model			Pseudo-second-order model				
	Q_e (mg g^{-1})	K_1 (min^{-1})	R^2	Q_e (mg g^{-1})	K_2 (g mg^{-1} min^{-1})	h (mg g^{-1} min^{-1})	$t_{1/2}$ (min)	R^2
ZIF-90	4.72	3.46×10^{-2}	0.97	7.58	1.13×10^{-2}	0.65	11.67	0.99
ZIF-90-SO_2HN_2	7.14	3.02×10^{-2}	0.97	13.89	6.96×10^{-3}	1.34	10.34	0.99

(min). The calculation results of all parameters are listed in Table 1.

To explore the factors affecting the adsorption rate of ZIF-90 and ZIF-90-SO_2HN_2, the Boyd external diffusion rate control model and the Weber-Morris internal diffusion rate control model were used to analyze the experimental results. The Boyd model assumes that the resistance to diffusion mainly comes from the liquid film generated on the particle surface, and the calculation formula is as follows [44]:

$$B_t = K_B t + I_B \tag{6}$$

$$B_t = -0.4977 - \ln\left(1 - \frac{Q_t}{Q_e}\right) \tag{7}$$

where B_t is the function of Q_t/Q_e; K_B is the Boyd model constant (min^{-1}); I_B is the intercept of the Boyd model. The closer the value of I_B is to 0, the stronger the dominant role of liquid film diffusion in the adsorption process.

The Weber–Morris model assumes that the resistance of liquid film diffusion is negligible or only works for a very short time at the beginning of adsorption, the diffusion coefficient is constant and the direction of adsorbate diffusion is random [45]. Its calculation formula is as follows [46]:

$$Q_t = I_W + K_W t^{1/2} \tag{8}$$

where I_W is the intercept of the Weber–Morris model; K_W is the diffusion rate constant (mg g^{-1} $min^{-1/2}$). The larger the value of I_W, the greater the liquid film resistance. When $I_W = 0$, the liquid film resistance can be ignored.

The fitting results of the two models are shown in Fig. 10 and Table 2. The correlation coefficient R^2 of the Boyd model is larger than that of the Weber–Morris model, indicating that the adsorption of Co(II) on ZIF-90 and ZIF-90-SO_2HN_2 is more in line with the Boyd model. In addition, the I_B values of the two adsorbents are −0.11 and 0.10, respectively, which fully indicates that the influence of liquid film diffusion on the adsorption rate is dominant in the entire adsorption process. Most of the adsorbate is adsorbed by the outer surface after passing through the liquid film on the surface of the adsorbents.

Effect of temperature and initial ion concentration

Figure 11 shows the curves of the adsorption capacity of ZIF-90 and ZIF-90-SO_2HN_2 for Co(II) at different temperatures as a function of the initial concentration of the solution. With the increase of the initial concentration of the solution, the adsorption capacity of ZIF-90 and ZIF-90-SO_2HN_2 for Co(II) also increased rapidly, and the two adsorbents basically reached the maximum adsorption capacity when the Co(II) concentration was about 250 mg L^{-1}. The maximum

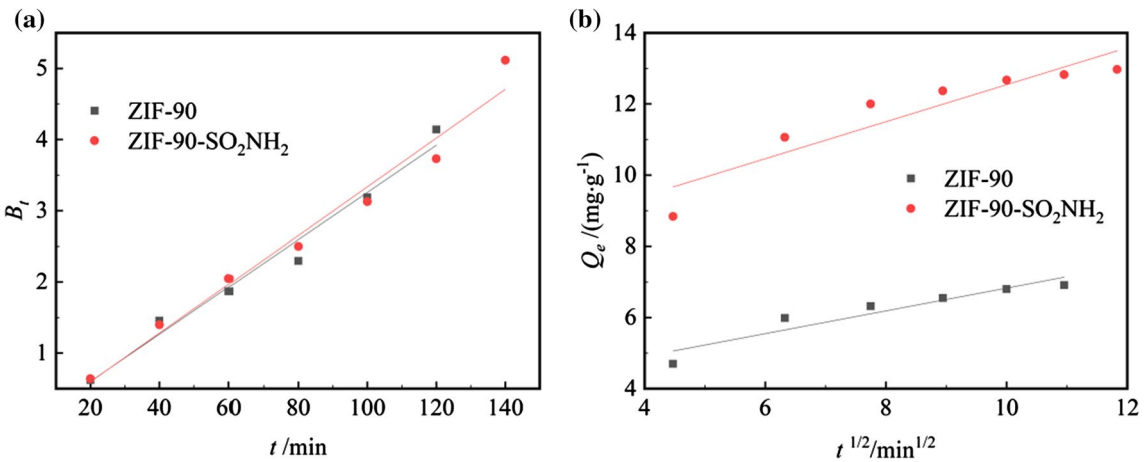

Fig. 10 Boyd model (**a**) and Weber–Morris model (**b**) fitting of ZIF-90 and ZIF-90-SO_2HN_2 (pH = 6.67, T = 303 K, initial Co(II) concentration of 10 mg L^{-1})

Table 2 Parameters calculated by Boyd model and Weber-Morris model (pH = 6.67, T = 303 K, initial Co(II) concentration of 10 mg L^{-1})

Kind of adsorbent	Boyd model			Weber–Morris model		
	K_B (min^{-1})	I_B	R^2	K_W (mg g^{-1} $min^{-0.5}$)	I_W (mg g^{-1})	R^2
ZIF-90	3.46×10^{-2}	−0.11	0.97	0.40	4.83	0.82
ZIF-90-SO_2HN_2	3.02×10^{-2}	0.10	0.97	0.51	7.40	0.85

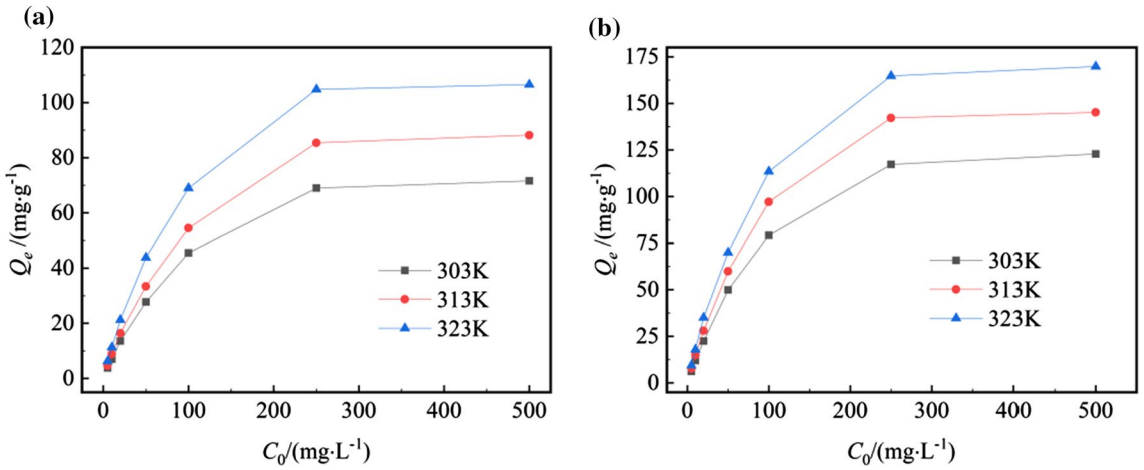

Fig. 11 Effect of initial concentration on adsorption capacity of ZIF-90 (**a**) and ZIF-90-SO_2HN_2 (**b**) at different temperatures (pH = 6.72, t = 720 min)

adsorption capacity of ZIF-90 is 74.60 mg g^{-1}, and that of ZIF-90-SO_2HN_2 is 122.85 mg g^{-1}.

To analyze the characteristics of ZIF-90 and ZIF-90-SO_2HN_2 adsorption process of Co(II), Langmuir, Freundlich and Dubinin–Radushkevich three isotherm adsorption models were used to analyze the experimental results.

The Langmuir model assumes that there is no interaction between the adsorbed molecules, the active sites on the adsorbent surface are uniformly distributed and the adsorption is monolayer [47]:

$$\frac{C_e}{Q_e} = \frac{C_e}{Q_m} + \frac{1}{K_L Q_m} \tag{9}$$

where C_e is the concentration of Co(II) when it reaches the adsorption equilibrium (mg L^{-1}); Q_m is the saturated adsorption capacity predicted by the Langmuir model (mg g^{-1}); K_L is the Langmuir adsorption equilibrium constant (L mg^{-1}).

The Freundlich model proposes an empirical model based on heterogeneous surface adsorption, assuming that the adsorbent has a non-uniform surface with non-uniform energy of active adsorption sites [48]:

$$\ln Q_e = \ln K_F + \frac{1}{n} \ln C_e \tag{10}$$

where K_F is the Freundlich adsorption equilibrium constant (mg g^{-1}); n is the adsorption constant of Freundlich model. When n = 2–10, the adsorption process is easy to occur, but when $n \leq 0.5$, the adsorption process is difficult to occur [49].

The Dubinin-Radushkevich model assumes that adsorption is the process by which the adsorbate fills the pores of the adsorbent, providing information on the physical or chemical mechanism of the adsorption process [50]:

$$Q_e = Q_{DR} \exp\left(-K_{DR} \varepsilon^2\right) \tag{11}$$

$$\varepsilon = RT \ln\left(1 + \frac{1}{C_e}\right) \tag{12}$$

where Q_{DR} is the maximum adsorption capacity of the adsorbent calculated by the Dubinin-Radushkevich model (mg g^{-1}); K_{DR} is the adsorption isotherm constant of the Dubinin-Radushkevich model (mol^2 kJ^{-2}); ε is the Polanyi potential energy of the adsorbent (J mol^{-1}). The free adsorption energy E (kJ mol^{-1}) can be calculated from the K_{DR} value. When $E \leq 8$ kJ mol^{-1}, the adsorption process is a physical process; and when $E > 8$ kJ mol^{-1}, the adsorption process is a chemical process. Its calculation formula is as follows [51]:

$$E = \frac{1}{\sqrt{2K_{DR}}} \tag{13}$$

At 303 K, the fitting results and calculation parameters are shown in Fig. 12 and Table 3. The correlation coefficient R^2 of the Langmuir isotherm is greater than that of the Freundlich isotherm and the Dubinin-Radushkevich isotherm. This proves that the active sites on the ZIF-90 and ZIF-90-SO_2HN_2 surfaces are uniformly distributed and Co(II) is adsorbed in a monolayer on the surface of the adsorbent. In the Freundlich model, the adsorption constants n are all larger than 2, indicating that the adsorption process easily occurs in the absence of an external driving force. In the Dubinin–Radushkevich model, the free adsorption energy E values of two adsorbents are larger than 8 kJ mol^{-1}, which proves that the adsorption process is a chemical process.

In addition, the separation coefficient R_L, which reflects the affinity of ZIF-90-SO_2HN_2 for solutes, can be

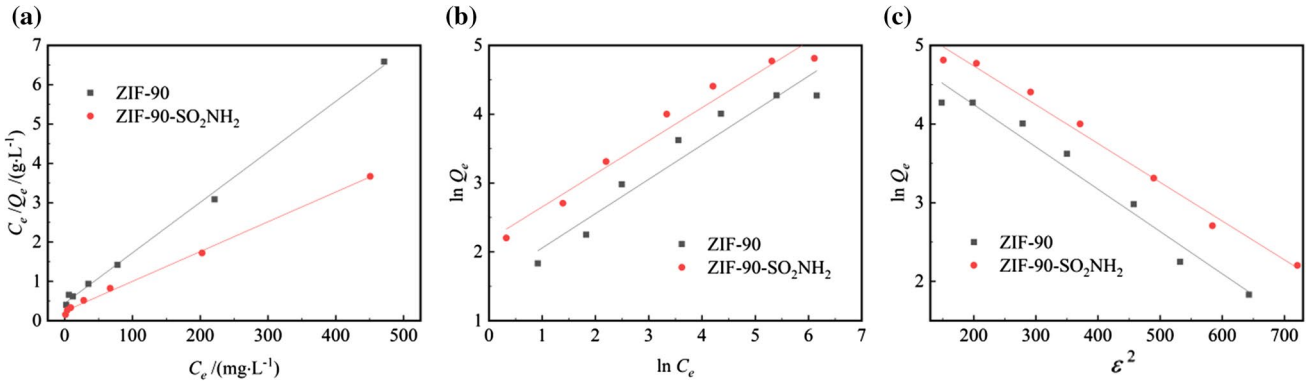

Fig. 12 Fitting of Langmuir (**a**), Freundlich (**b**) and Dubinin–Radushkevich (**c**) isotherms for the adsorption of Co(II) at 303 K (pH = 6.72, t = 720 min)

Table 3 Fitting parameters of three isothermal adsorption models (pH = 6.72, t = 720 min)

Isotherm models	Parameters	ZIF-90	ZIF-90-SO_2HN_2
Langmuir isotherm	Q_m (mg g^{-1})	78.13	131.58
	K_L(L mg^{-1})	2.90×10^{-2}	3.15×10^{-2}
	R^2	0.99	0.99
Freundlich isotherm	K_F ((mg g)(L $mg^{-1})^{1/n}$)	4.74	8.79
	n	2.00	2.08
	R^2	0.93	0.96
Dubinin-Radushkevich isotherm	Q_{DR} (mg g^{-1})	205.00	306.37
	K_{DR} (mol^2 kJ^{-2})	5.40×10^{-3}	4.90×10^{-3}
	E(kJ mol^{-1})	9.62	10.10
	R^2	0.97	0.98

calculated according to the equilibrium constant K_L in the Langmuir model, and its calculation formula is [52]:

$$R_L = \frac{1}{1 + K_L C_0} \tag{14}$$

When $R_L = 0$, the adsorption process is irreversible; when $0 < R_L < 1$, it is favorable for the adsorption process, and the smaller the R_L value, the more favorable the adsorption occurs; when $R_L = 1$, the adsorption process is linear adsorption; when $R_L > 1$, the adsorption process is unfavorable. The variation of R_L with the initial concentration of Co(II) is shown in Fig. 13. It can be found that the R_L value on the curve is always less than 1 and gradually decreases as the solution concentration increases, which proves that the adsorption of Co(II) by ZIF-90-SO_2HN_2 is easier to occur with the increase of solution concentration.

The data in Fig. 11 show that the equilibrium adsorption capacity of ZIF-90-SO_2HN_2 for Co(II) gradually increases with increasing temperature, indicating that the adsorption is endothermic. To understand the effect of temperature on the adsorption performance of ZIF-90-SO_2HN_2, the

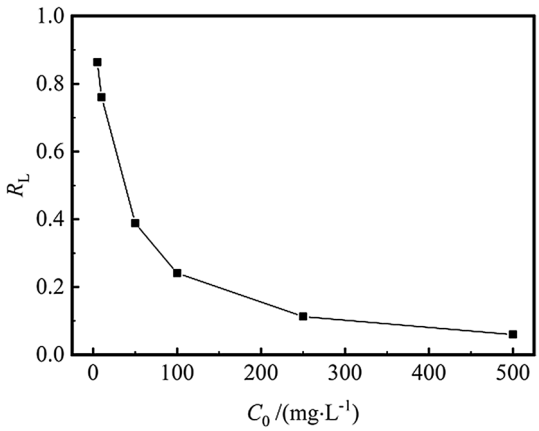

Fig. 13 Separation coefficient R_L of ZIF-90-SO_2HN_2 for Co(II) at different concentrations (pH = 6.72, t = 720 min)

experimental results were thermodynamically analyzed by the following equation [53]:

$$\ln K_d = \frac{\Delta S^0}{R} - \frac{\Delta H^0}{RT} \tag{15}$$

$$\Delta G^0 = \Delta H^0 - T\Delta S^0 \tag{16}$$

$$K_d = \frac{Q_e}{C_e} = \frac{(C_0 - C_e)}{C_e}\frac{V}{m} \tag{17}$$

where: K_d is the distribution coefficient of Co(II) (mL g^{-1}); T is the absolute temperature (K); R is the ideal gas constant, usually assigned as 8.314 J mol^{-1} K^{-1}. ΔS^0 is the standard entropy change (J mol^{-1} K^{-1}); ΔH^0 is the standard enthalpy change (kJ mol^{-1}); ΔG^0 is the change in Gibbs free energy (kJ mol^{-1}). The values of ΔH^0 and ΔS^0 can be calculated from the slope and intercept of the linear regression of $\ln K_d$ versus $1/T$ in Fig. 14 [54].

The adsorption thermodynamic parameters of ZIF-90-SO_2HN_2 for Co(II) at different temperatures are listed in Table 4. The positive value of ΔH^0 indicates that the adsorption process of Co(II) by ZIF-90-SO_2HN_2 is endothermic in nature. The negative value of ΔG^0 indicates that the adsorption process is feasible and spontaneous. The decrease in the value of ΔG^0 with increasing temperature proves that the adsorption process is more efficient at higher temperatures [55].

Table 4 Adsorption thermodynamic parameters of Co(II) on ZIF-90-SO_2HN_2 (pH = 6.72, t = 720 min)

Temperature (K)	K_d	ΔG^0 (kJ mol^{-1})	ΔH^0 (kJ mol^{-1})	ΔS^0 (J mol^{-1} K^{-1})
303	1.02	−0.06		
313	1.51	−1.06	30.35	100.36
323	2.15	−2.07		

Effect of co-existing ions

In the actual wastewater produced by nuclear facilities, there are usually non-radioactive ions such as K(I), Na(I), Ca(II), Mg(II) and radioactive metal ions such as Sr(II), Mn(II), Cs(I), Ni(II). To evaluate the selective adsorption performance of ZIF-90 and ZIF-90-SO_2HN_2, 0.02 g adsorbents were added to the multi-component solution which had the same concentration (10 mg L^{-1}) of K(I), Na(I), Ca(II), Mg(II), Sr(II), Co(II), Mn(II), Cs(I), Ni(II). The experimental results are shown in Fig. 15. It can be seen that ZIF-90-SO_2HN_2 has stronger selective adsorption capacity for Co(II) and Ni(II) than ZIF-90, and the adsorption capacities are 10.26 mg g^{-1} and 8.28 mg g^{-1}, respectively. The adsorption capacities of Mn(II), Ca(II), Mg(II) and Sr(II) all decreased to varying degrees, which may be because the sulfonamide group had better affinity for metal ions such as Co(II) and Ni(II), which belonged to boundary acids. Moreover, ZIF-90 and ZIF-90-SO_2HN_2 have almost no adsorption effect on K(I), Na(I) and Cs(I), which may be due to the lack of binding sites for monovalent metal ions on the surface of the two adsorbents.

Comparison of performance between ZIF-90-SO_2HN_2 and other adsorbents

The adsorption properties of ZIF-90-SO_2HN_2 and other adsorbents for Co(II) are compared in Table 5. Compared with most adsorbents, ZIF-90-SO_2HN_2 has a shorter equilibrium adsorption time for Co(II), which is due to the hydrophilicity of the material itself. At the same time, ZIF-90-SO_2HN_2 has higher adsorption capacity for Co(II) than most adsorbents, which is beneficial for waste minimization.

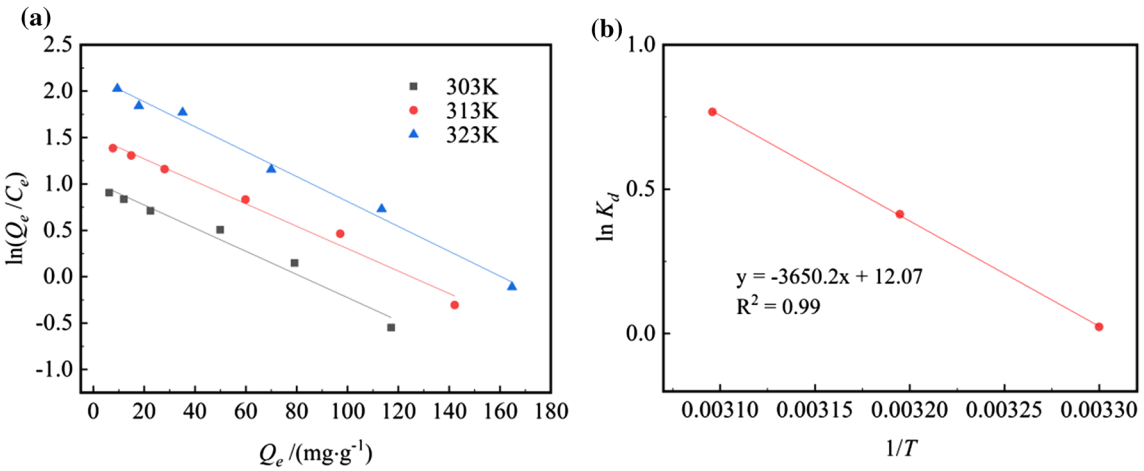

Fig. 14 Khan plots of ZIF-90-SO_2HN_2 for Co(II) adsorption at different temperatures (**a**) and relationship curve between $\ln K_d$ and $1/T$ (**b**) (pH = 6.72, t = 720 min)

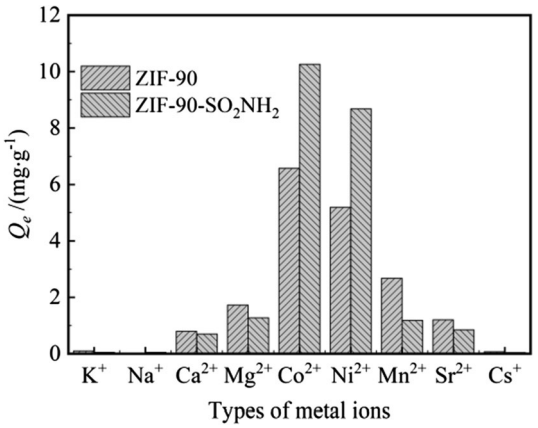

Fig. 15 The adsorption capacity of ZIF-90 and ZIF-90-SO_2HN_2 for co-existing metal ions (pH = 6.72, t = 720 min)

Conclusion

In this study, a sulfonamide-functionalized ZIF adsorbent was successfully synthesized for the efficient extraction of cobalt ions from solution. The obtained ZIF-90-SO_2HN_2 has an average particle size of less than 1 μm with a microporous structure and good thermal stability at 300 °C. The maximum adsorption capacity of ZIF-90-SO_2HN_2 for Co(II) is 122.85 mg g^{-1} under the conditions of pH = 6.72 and T = 303 K. The initial concentration of the solution is 250 mg L^{-1}, which is significantly higher than that of pristine ZIF-90. The Lagergren pseudo-second-order kinetic model and Langmuir adsorption isotherm model are more in line with the adsorption process of ZIF-90-SO_2HN_2 for Co(II), which indicates that the surface active sites of ZIF-90-SO_2HN_2 are uniformly distributed, and the adsorption of Co(II) is a monolayer chemisorption. ZIF-90-SO_2HN_2 has good selective adsorption for both Co(II) and Ni(II) in multi-metal ion solution. Due to the excellent hydrophilic properties of ZIF-90, the sulfonamide-modified material ZIF-90-SO_2HN_2 has a good application prospect in the rapid adsorption of Co(II) and Ni(II) in solution.

Acknowledgements The work described in this paper was fully supported by a Grant from the National Natural Science Foundation of China (No. 51573208).

Declarations

Conflict of interest There no conflicts of interest to declare.

References

1. Manohar DM, Noeline BF, Anirudhan TS (2006) Adsorption performance of Al-pillared bentonite clay for the removal of cobalt(II) from aqueous phase. Appl Clay Sci 31(3/4):194–206
2. Siva S, Sudharsan S, Kannan RS (2015) Selective Co(II) removal from aqueous media by immobilizing silver nanoparticles within a polymer-matrix through a formaldehyde cross linking agent. RSC Adv 5:23340–23349
3. Yuan G, Tu H, Li M, Liu J, Zhao C, Liao J, Yang Y, Yang J, Liu N (2018) Glycine derivative-functionalized metal–organic framework (MOF) materials for Co(II) removal from aqueous solution. Appl Surf Sci 466:903–910
4. Fang F, Kong L, Huang J, Wu S, Zhang K, Wang X, Sun B, Jin Z, Wang J, Huang XJ, Liu J (2014) Removal of cobalt ions from aqueous solution by an amination graphene oxide nanocomposite. J Hazard Mater 270:1–10
5. Barakat MA (2011) New trends in removing heavy metals from industrial wastewater. Arab J Chem 4(4):361–377
6. Narin I, Soylak M (2003) Enrichment and determinations of nickel(II), cadmium(II), copper(II), cobalt(II) and lead(II) ions in natural waters, table salts, tea and urine samples as pyrrolydine dithiocarbamate chelates by membrane filtration-flame atomic absorption spectrometry C. Anal Chim Acta 493(2):205–212
7. Piscureanu A, Chican I, Varasteanu D, Dulama M, Ruse M (2015) Aspects concerning the selection of ion exchange resin for low level radwaste waters decontamination. Revista de Chimie -Bucharest- Original Edition- 66(11):1819–1825
8. Wang Y, Ye G, Chen H, Hu X, Niu Z, Ma S (2015) Functionalized metal-organic framework as a new platform for efficient and selective removal of cadmium(II) from aqueous solution. J Mater Chem A 3(29):15292–15298
9. Thiebault T, Brendlé J, Auge G, Limousy L (2020) Cleaner synthesis of silylated clay minerals for the durable recovery of

Table 5 Comparison of performance between ZIF-90-SO_2HN_2 and other adsorbents

Types of adsorbents	Maximum adsorption capacity (mg g^{-1})	Adsorption equilibrium time (min)	References
Ammoxidized graphene oxide nanocomposites	116.35	20	[4]
Imprinted UiO-66-NH_2	175.00	900	[12]
Arginine-functionalized MgAl-NO_3-LDH	68.95	1500	[56]
Imprinted silica Co(II)-IIP	106.00	180	[57]
MIL-100(Fe)	119.00	390	[58]
Porous chelating resin	71.29	345	[59]
chitosan grafted with EDTA	61.00	250	[60]
ZIF-90-SO_2HN_2	122.85	120	This study

ions (Co^{2+} and Sr^{2+}) from aqueous solutions. Ind Eng Chem Res 59(5):2104–2112
10. Bordoloi N, Goswami R, Kumar M, Kataki R (2017) Biosorption of Co(II) from aqueous solution using algal biochar: KINETICS and isotherm studies. Biores Technol 2017:1465–1465
11. El-Zahhar AA, Abdel-Aziz HM, Siyam T (2006) Some synthesized polymeric composite resins for the removal of Co(II) and Eu(III) from aqueous solutions. J Radioanal Nucl Chem 267(3):657–664
12. Yuan GY, Tu H, Liu J, Zhao C, Liao J, Yang Y, Yang J, Ning L (2018) A novel ion-imprinted polymer induced by the glycylglycine modified metal-organic framework for the selective removal of Co(II) from aqueous solutions. Chem Eng J 333(1):280–288
13. Ryan JK, Daren JT, Fang QR, Li JR, Trevor AM, Mark DY, Yuan DQ, Zhao D, Zhuang WJ, Zhou HC (2009) Potential applications of metal–organic frameworks. Coord Chem Rev 253(23–24):3042–3066
14. Eddaoudi M (2002) Systematic design of pore size and functionality in isoreticular MOFs and their application in methane storage. Science 295(5554):469–472
15. Yu Z, Deschamps J, Hamon L, Prabhakaran PK, Pre P (2017) Hydrogen adsorption and kinetics in MIL-101(Cr) and hybrid activated carbon-MIL-101(Cr) materials. Int J Hydrogen Energy 42(12):8021–8031
16. Cunha D, Yahia MB, Hall S, Miller SR, Chevreau H, Elka ME (2013) Rationale of drug encapsulation and release from biocompatible porous metal–organic frameworks. Chem Mater 25(14):2767–2776
17. Taylor PK, Rocca JD, Xie Z, Tran S, Lin W (2009) Postsynthetic modifications of iron-carboxylate nanoscale metal–organic frameworks for imaging and drug delivery. J Am Chem Soc 131(40):14261–14263
18. Li B, Zhang Y, Ma D, Lu L, Li G, Li G (2012) A strategy toward constructing a bifunctionalized mof catalyst: post-synthetic modification of MOFs on organic ligands and coordinatively unsaturated metal sites. Chem Commun 48(49):6151–6153
19. Wu CD, Hu AG, Lin Z, Lin WB (2005) A homochiral porous metal–organic framework for highly enantioselective heterogeneous asymmetric catalysis. J Am Chem Soc 127(25):8940–8941
20. Hu Z, Deibert BJ, Li J (2014) Luminescent metal–organic frameworks for chemical sensing and explosive detection. Chem Soc Rev 43(16):5815–5840
21. Dalapati R, Biswas S (2017) Post-synthetic modification of a metal–organic framework with fluorescent-tag for dual naked-eye sensing in aqueous medium. Sens Actuators B Chem 239:759–767
22. Qu F, Xia L, Wu C, Liu L, Li G, You J (2016) Sensitive and accurate determination of sialic acids in serum with the aid of dispersive solid-phase extraction using the zirconium-based MOF of UIO-66-NH_2 as sorbent. RSC Adv 6(69):64895–64901
23. Esrafili L, Safarifard V, Tahmasebi E, Esrafili MD, Morsali A (2018) Functional group effect of isoreticular metal–organic frameworks on heavy metal ion adsorption. New J Chem 42:8864–8873
24. Anh P, Christian JD, Fernando JUR, Carolyn BK, Michael OK, Omar MY (2010) Synthesis, structure, and carbon dioxide capture properties of zeolitic imidazolate frameworks. Acc Chem Res 43(1):58–67
25. Calero S, Gómez-Álvarez P (2015) Underlying adsorption mechanisms of water in hydrophobic and hydrophilic zeolite imidazolate frameworks: ZIF-71 and ZIF-90. J Phys Chem C 119:23774–23780
26. Yuan GY, Tian Y, Liu J, Tu H, Liao J, Yang J (2017) Schiff base anchored on metal–organic framework for Co(II) removal from aqueous solution. Chem Eng J 326:691–699
27. Qin X, Yang W, Yang W, Ma Y, Pan Q (2021) Covalent modification of ZIF-90 for uranium adsorption from seawater. Microporous Mesoporous Mater 323:111231
28. Bhattacharjee S, Lee YR, Ahn WS (2015) Post-synthesis functionalization of a zeolitic imidazolate structure ZIF-90: a study on removal of Hg(II) from water and epoxidation of alkenes. CrystEngComm 17(12):2575–2582
29. Yang MH, Duan CX, Zeng XJ, Li JJ, Liu CY, Zeng LJ, Zhang Y, Wang K, Xi HX (2021) Facile fabrication of nanoscale hierarchical porous zeolitic imidazolate frameworks for enhanced toluene adsorption capacity. Rare Met 40(2):471–477
30. Yang T, Chung TS (2013) Room-temperature synthesis of ZIF-90 nanocrystals and the derived nano-composite membranes for hydrogen separation. J Mater Chem A 1(19):6081–6090
31. Kursunlu AN, Guler E, Sevgi F, Ozkalp B (2013) Synthesis, spectroscopic characterization and antimicrobial studies of Co(II), Ni(II), Cu(II) and Zn(II) complexes with Schiff bases derived from 5-bromo-salicylaldehyde. J Mol Struct 1048:476–481
32. Kursunlu AN, Guler E, Dumrul H, Kocyigit O, Gubbuk IH (2009) Chemical modification of silica gel with synthesized new Schiff base derivatives and sorption studies of cobalt(II) and nickel(II). Appl Surf Sci 255:8798–8803
33. Lopachin RM, Gavin T, Decaprio A, Barber DS (2012) Application of the hard and soft, acids and bases (HSAB) theory to toxicant-target interactions. Chem Res Toxicol 25(2):239–251
34. Shieh FK, Wang SC, Leo SY, Kevin WuCW (2013) Water-based synthesis of zeolitic imidazolate framework-90 (ZIF-90) with a controllable particle size. Chem-A Eur J 19:11139–11142
35. Hu ZG, Peng YW, Kang ZX, Qian YH, Zhao D (2015) A modulated hydrothermal (MHT) approach for the facile synthesis of UIO-66-Type MOFs. Inorg Chem 54(10):4862–4868
36. Zhou Y, Wang X, Men J, Jia M, Liang C (2022) Study on the adsorption performance of zeolitic imidazolate framework-8 (ZIF-8) for Co^{2+} and Mn^{2+}. J Radioanal Nucl Chem 331(3):1367–1379
37. Mei D, Li H, Liu L, Jiang L, Ma F (2021) Efficient uranium adsorbent with antimicrobial function: oxime functionalized ZIF-90. Chem Eng J 425(1):130468–130479
38. Morris W, Doonan CJ, Furukawa H, Banerjee R, Yaghi OM (2008) Crystals as molecules: postsynthesis covalent functionalization of zeolitic imidazolate frameworks. J Am Chem Soc 130:12626–12627
39. Jose T, Hwang Y, Kim DW, Kim MI, Park DW (2015) Functionalized zeolitic imidazolate framework F-ZIF-90 as efficient catalyst for the cycloaddition of carbon dioxide to allyl glycidyl ether. Catal Today 245:61–67
40. Xie W, Wan F (2019) Guanidine post-functionalized crystalline ZIF-90 frameworks as a promising recyclable catalyst for the production of biodiesel via soybean oil transesterification. Energy Convers Manag 198:111922
41. Simons WW (1978) The Sadtler handbook of infrared spectra. Sadtler Research Laboratories
42. Guo WL, Chen R, Liu Y, Meng MJ, Meng XG, Hu ZY, Song ZL (2013) Preparation of ion-imprinted mesoporous silica SBA-15 functionalized with triglycine for selective adsorption of Co(II). Colloids Surf A 436(35):693–703
43. Altinisik A, Gür E, Seki Y (2010) A natural sorbent, lufa cylindrica for the removal of a model basic dye. J Hazard Mater 179(1–3):658–664
44. Rui MCV, Campinas M, Costa H, Rosa MJ (2014) How do the hsdm and boyd's model compare for estimating intraparticle difusion coefcients in adsorption processes. Adsorption 20(5–6):737–746
45. Liang CQ, Jia MC, Wang XW, Du ZH, Ding H (2019) Preparation of potassium niobium sulfide and its selective adsorption properties for Sr^{2+} and Co^{2+}. J Radioanal Nucl Chem 322(12):1–11

46. Hassanzadeh M, Ghaemy M (2018) Preparation of bio-based keratin-derived magnetic molecularly imprinted polymer nanoparticles for the facile and selective separation of bisphenol a from water. J Sep Sci 41(10):2296–2304
47. Yin CY, Aroua MK, Daud WMAW (2007) Impregnation of palm shell activated carbon with polyethyleneimine and its effects on Cd^{2+} adsorption. Colloid Surf A 307(1–3):128–136
48. Ajenifuja E, Ajao JA, Ajayi EOB (2017) Equilibrium adsorption isotherm studies of Cu(II) and Co(II) in high concentration aqueous solutions on Ag-TiO_2-modifed kaolinite ceramic adsorbents. Appl Water Sci 7(5):2279–2286
49. Li H, Cao X, Zhang C, Yu Q, Zhao Z, Niu X (2017) Enhanced adsorptive removal of anionic and cationic dyes from single or mixed dye solutions using MOF PCN-222. RSC Adv 7(27):16273–16281
50. Zahakifar F, Keshtkar AR, Talebi M (2020) Performance evaluation of sodium alginate/polyvinyl alcohol/polyethylene oxide/ZSM5 zeolite hybrid adsorbent for ion uptake from aqueous solutions: a case study of thorium(IV). J Radioanal Nucl Chem 327(3):65–72
51. Alamdarlo FV, Solookinejad G, Zahakifar F, Jalal MR, Jabbari M (2021) Study of kinetic, thermodynamic, and isotherm of Sr adsorption from aqueous solutions on graphene oxide (GO) and (aminomethyl) phosphonic acid-graphene oxide (AMPA-GO). J Radioanal Nucl Chem 329(2):1033–1043
52. Crini G (2005) Recent developments in polysaccharide-based materials used as adsorbents in wastewater treatment. Prog Polym Sci 30(1):38–70
53. Zahakifar F, Keshtkar AR, Talebi M (2021) Synthesis of sodium alginate (SA)/polyvinyl alcohol (PVA)/polyethylene oxide (PEO)/ZSM-5 zeolite hybrid nanostructure adsorbent by casting method for uranium(VI) adsorption from aqueous solutions. Prog Nucl Energy 134:103642
54. Khan AA, Singh RP (1987) Adsorption thermodynamics of carbofuran on Sn(IV) arsenosilicate in H^+, Na^+ and Ca^{2+} forms. Colloids Surf 24(1):33–42
55. Xing M, Wang J (2016) Nanoscaled zero valent iron/graphene composite as an efficient adsorbent for Co(II) removal from aqueous solution. J Colloid Interface 474:119–128
56. Pka B, Rk C, Ks A (2019) Arginine and lysine-functionalized layered double hydroxides as efficient sorbents for radioactive Co^{2+} removal by chelate-facilitated immobilization. Chem Eng J 374:359–369
57. Liu Y, Zhong G, Liu Z, Meng M, Jiang Y, Ni L, Guo W, Liu F (2015) Preparation of core-shell ion imprinted nanoparticles via photoinitiated polymerization at ambient temperature for dynamic removal of cobalt in aqueous solution. RSC Adv 104(5):85691–85704
58. Moghadam RM, Khosravi NMR, Anvaripour B (2018) Equilibrium, kinetics and thermodynamics studies on adsorptive removal of cobalt ions from wastewater using MIL-100(Fe). Int J Sustain Eng 12(2):1–10
59. Cegłowski M, Schroeder G (2015) Preparation of porous resin with Schiff base chelating groups for removal of heavy metal ions from aqueous solutions. Chem Eng J 263:402–411
60. Zhuang S, Zhang Q, Wang J (2020) Adsorption of Co^{2+} and Sr^{2+} from aqueous solution by chitosan grafted with EDTA. J Mol Liq 325(3):115197